Chapter 3

DETECTION OF DRILL-BIT SIGNAL

3.1 Introduction

The goal in this chapter is to detect the drill-bit signal from measurements of its moveout across the horizontal and vertical seismic arrays in the OGS experiment. The moveout of compressional waves generated by the drill bit should be well approximated by hyperbolic traveltime curves (Equation 2.3.3), because the subsurface in the OGS experiment is horizontally layered (OGS, 1988).

To identify the drill-bit signal, I compare the moveout measured from the data to the moveout predicted by the hyperbolic traveltime model, knowing the depth of the drill-bit source and the stacking velocities from a surface seismic survey (Appendix B). These two measures of moveout will agree over an interval of borehole depths only if the events in the data are direct arrivals from the drill bit. It is unlikely that the moveout of events unrelated to the drill bit will change consistently as the depth of the borehole increases. As for measurements of moveout from a single depth level, at least two 1-D arrays are needed in order to discriminate between sources at depth and sources at the surface (Figure 3.1).

Poor signal-to-noise ratio is the main issue when measuring moveout from seismic data recorded during drilling. Therefore, I estimate the moveout by stacking along presumed trajectories of coherency, rather than by cross-correlation of adjacent traces. The stacking trajectories are defined by three parameters — zero-offset time, velocity and depth. The reason for introducing an additional parameter with respect to the conventional velocity analysis of surface seismic data is that for non-impulsive sources such as the drill bit, the time on the zero-offset trace is no longer the ratio of depth and velocity. The 3-D

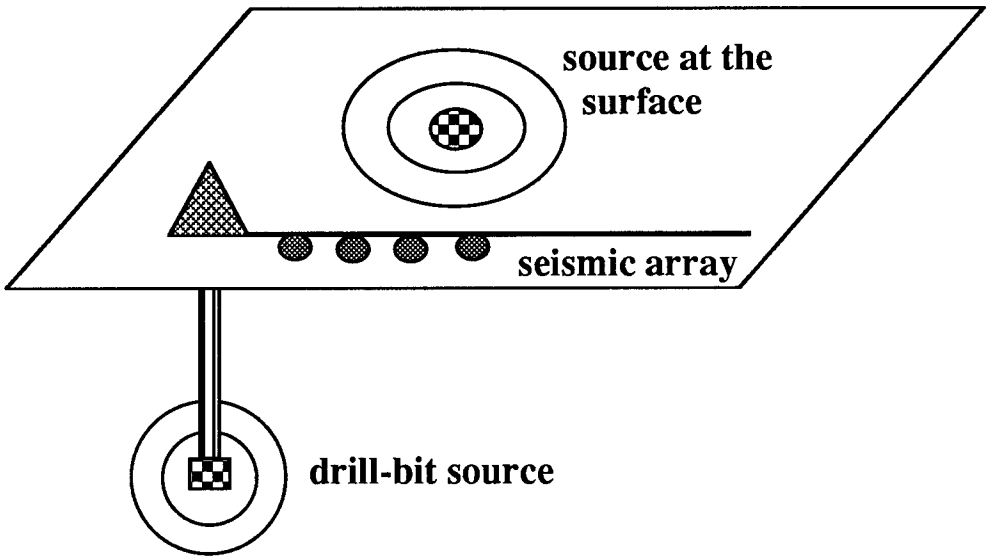

FIG. 3.1. A source at depth and a source at the surface may have similar traveltime delays (moveout) across a 1-D array of vertical-component geophones, even though the velocities of propagation in the direction *perpendicular* to the array differ significantly. Conversely, there is an ambiguity in determining the position of the source from 1-D, single-component data.

velocity spectrum obtained by stacking the drill-bit data can be searched in several ways for coherent events. For instance, the 2-D velocity panel of conventional velocity analysis for surface seismic data is a slice of this 3-D velocity spectrum. I discuss issues related to the computation of such velocity spectra in Appendixes C and D.

To improve the signal-to-noise ratio, and thereby the results of the velocity analysis, I cross-correlate the data with a "reference" signal from a geophone at depth. Using a model for the signal and noise, I argue that averaging cross-correlated seismograms should compress the drill-bit waveform into a short time-window where locally the signal-to-noise ratio will be increased. Other methods for noise attenuation that could, and perhaps need to be used in conjunction with cross-correlation include velocity filtering of the surface seismic data, and editing and weighting of the noisy cross-correlated seismograms before computing their average.

The material in this chapter is organized in three parts. After defining the velocity spectra for non-impulsive sources, I compute such spectra from the surface array data. These spectra demonstrate that the strongest source in the data is not the drill bit, and

is most likely located at the surface. The drill-bit signal is not detected on such spectra because its power is, on average, smaller than the power of background noise with broadband spectrum of dips. In the second part, I enhance the drill-bit signal by cross-correlation and stacking of cross-correlated seismograms. Velocity analysis applied to the stacked seismogram detects an event with the characteristics expected for a direct arrival from the drill-bit source. The third part of the chapter contains a summary of results and recommendations for future experiments.

3.1.1 Definition of a velocity transform

For data recorded in an experiment with a non-impulsive source, I define a velocity transform by summing the data $d(t,x)$ along hyperbolic trajectories parametrized by depth z, velocity v and zero-offset traveltime t_0. Specifically, the value of the transform at (z,v,t_0) is given by:

$$V(z,v,t_0) = \sum_x d\left(x, t_0 + \frac{\sqrt{x^2 + z^2}}{v} - \frac{z}{v}\right). \tag{3.1}$$

The above definition assumes that the surface coordinates of the point-source are known and equal to the surface coordinates of the well. More generally, it could be necessary to scan also over ranges of parameters defining the surface location of the point-source (Cole, 1989).

The corresponding velocity spectrum is the square of the amplitude of the velocity transform, scaled by the inverse of the number of traces M:

$$S(z,v,t_0) = \frac{1}{M} \times |V(z,v,t_0)|^2 = \frac{1}{M} \times \left| \sum_x d\left(x, t_0 + \frac{\sqrt{x^2 + z^2}}{v} - \frac{z}{v}\right) \right|^2. \tag{3.2}$$

Coherent events with hyperbolic moveout in the time-offset domain will produce local maxima of energy in the 3-D velocity spectrum (Figure 3.2).

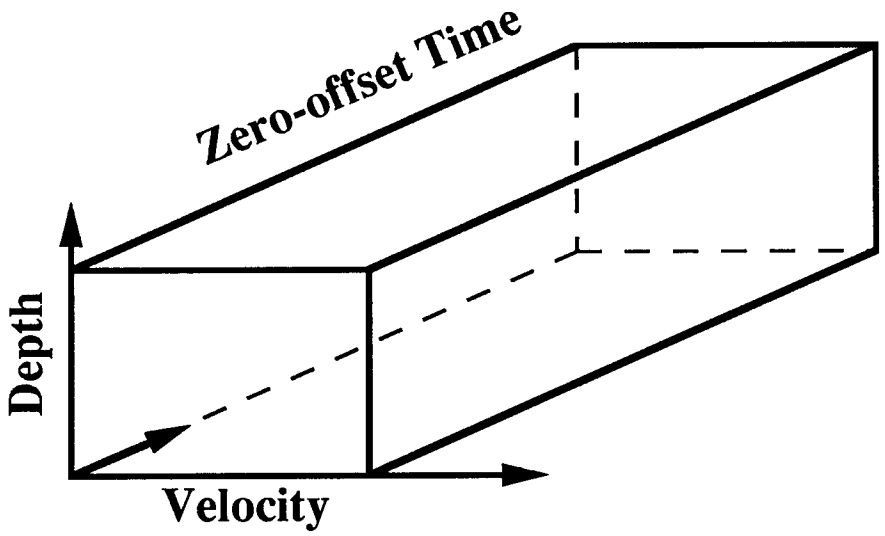

FIG. 3.2. The velocity transform for non-impulsive sources maps data recorded as a function of time, offset, and depth of the drill bit, into a 3-D space with coordinate axis zero-offset time, depth and velocity.

3.1.2 Measures of moveout: different views of the velocity cube

A point in velocity space: overlays of hyperbolas

A point in velocity space with coordinates (z, v, t_0) corresponds to a hyperbola in the time-offset domain. After the signal and noise separation applied in the previous chapter, a hyperbolic event is apparent in the data shown in Figure 3.3 (this same window of data was shown before processing in Figure 2.1). The moveout of this event is well approximated by an overlaid hyperbola whose parameters — depth equal to 0.9 km, and velocity equal to 3 km/s — differ significantly from the depth of the well (0.8 km) and from the stacking velocity (1.9 km/s) expected for a source at that depth. Such a discrepancy hints already that this strong event may not be generated by the drill-bit source (see also Figure 3.1). Further measurements of moveout will determine whether these events occur continuously in time and whether their moveout changes as the depth of the borehole increases.

Depth-velocity spectra

The computation of depth-velocity spectra, obtained by averaging over time the energy

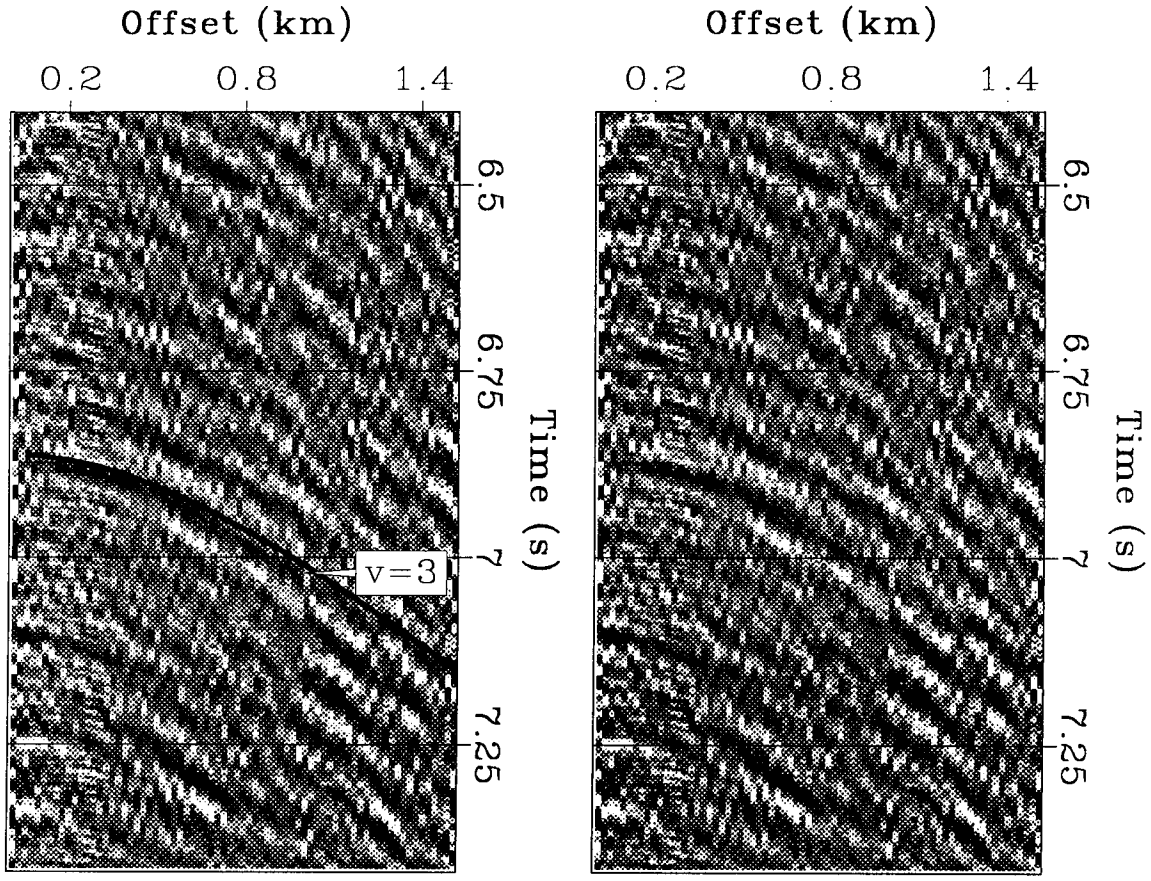

FIG. 3.3. Preliminary moveout analysis:
Left: Hyperbolas overlaid on data that have undergone the signal and noise separation process (Chapter 2).
Right: For comparison, the window of data on the left panel is redisplayed without the overlaid hyperbola.
The parameters of the hyperbola — depth of 0.9 km and velocity of 3 km/s — differ significantly from those expected for the signal from the drill-bit source.

in 3-D velocity spectra, provides a method for enhancing sources that operate continuously in time with respect to sources that are transient in time[1]. An expression for the energy in the depth-velocity spectrum, corresponding to parameters (z, v), and computed from a time-window of length T, is given by:

$$S(z,v) = \frac{1}{M \times T} \sum_{t_0=0}^{T} \left| \sum_{x} d\left(x, t_0 + \frac{\sqrt{x^2 + z^2}}{v} - \frac{z}{v} \right) \right|^2 ; \qquad (3.3)$$

Alternative expressions of the depth-velocity spectrum are derived in Appendix D in terms of the frequency components of the data, or of the spatial data-covariance matrix.

A depth-velocity spectrum, computed by averaging the energy along hyperbolic trajectories over a 10 min long period, is displayed in Figure 3.4. The main features of this spectrum are a ridge of large amplitudes, typical of the array response to a hyperbolic event (see also Figure B.3, page 69), and a background of uniform power. The peak value in that spectrum occurs for depth and velocity parameters consistent with those of the hyperbola overlaid in Figure 3.3; thus, the dominant source detected by this spectrum is not the drill-bit source. The ratio of the peak amplitude to the amplitude at the parameters expected for drill-bit signal (depth 0.8 km, velocity 1.9 km/s) is -3 db. In contrast, this ratio of amplitudes is -15 db, when computed from noiseless synthetic data, containing a single hyperbola with dominant frequency of 30 Hz (Figure B.3). The failure to detect the drill-bit source on the depth-velocity spectrum indicates that the power of that source is, on average, weaker than the background noise. On the other hand, interference from the strong source at the surface should not prevent the detection of the drill-bit signal, unless the drill-bit signal is weaker by at least -15 db.

Another depth-velocity spectrum, computed by averaging the energy in a 1 s long window of data (Figure 3.3), shows a local maximum of energy at the expected parameters for the drill-bit signal (Figure 3.5). The local maximum is about 3 db above the noise level, and about 3 db below the peak value in the spectrum, which is at the same parameters as the peak value in the average spectrum (Figure 3.4). The reason for which the background noise is weaker in that window of data may be related to either the drilling conditions, or to a better preliminary signal and noise separation. A further observation is that averaging

[1]A recent application of a similar time-dependent coherency analysis is the detection of a quarry blast from seismic data recorded with a 2-D array (Cole et al., 1989).

the spectrum over time cumulates signal as well as noise energy, and may degrade the signal-to-noise ratio.

In summary, the results from Figures 3.5 and 3.4 imply that at this stage of the processing there is dominant source at about 3 db above the background noise. The drill-bit signal on the other hand is weaker than the background noise, perhaps by no more than 3 db.

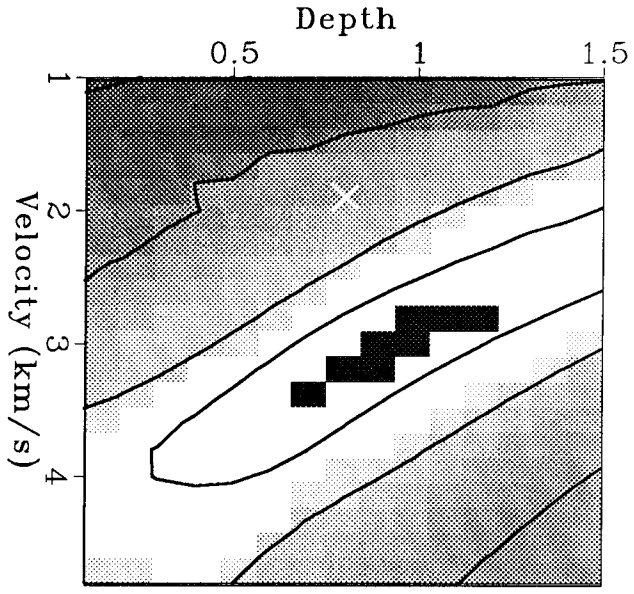

FIG. 3.4. Depth-velocity spectrum computed from a 10 min long sequence of data; the parameters of the dominant source (black squares) are significantly different from the expected parameters from the drill-bit signal (cross at depth of 0.8 km and velocity of 1.9 km/s).
The black squares indicate values in the stack above the 99^{th} percentile. Contours are at increments of 20% from the maximum value.

Time-velocity spectra

To detect changes in moveout that occur as a function of time in the 3-D velocity spectrum, while avoiding excessive computations, I compute the spectrum along a slanted plane corresponding to a constant ratio of depth and velocity. I choose that plane to be orthogonal to the ridge of maximum values seen on previous depth-velocity spectra (Figures 3.5 and 3.4), and generally orthogonal to the direction along which stacking trajectories yield the same power. In particular, I constrain the ratio of depth and velocity so that the plane intersects the region in the 3-D spectrum where the signal from the drill-bit is expected. Although such a slice through the 3-D spectrum may not contain the

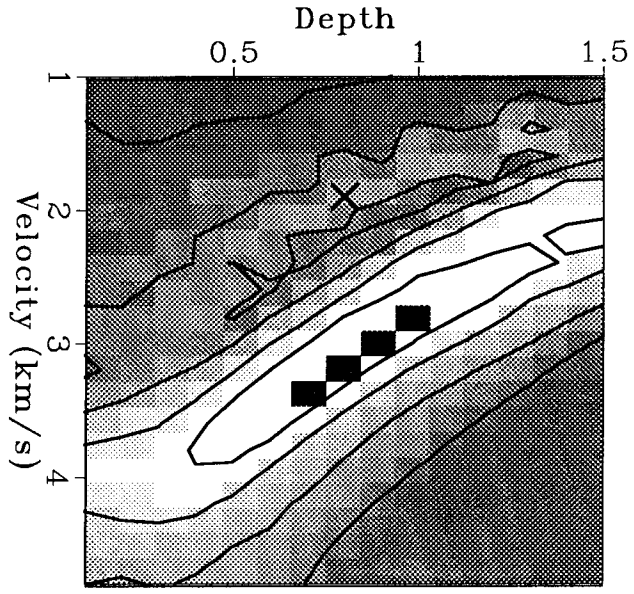

FIG. 3.5. Depth-velocity spectrum computed from a 1 s long window of data; the parameters of the dominant source (black squares) are significantly different from the expected parameters from the drill-bit signal (cross at depth of 0.8 km and velocity of 1.9 km/s).
The black squares indicate the largest values in the stack. Contours are at increments of 20% from the maximum value.

maxima of the power for each zero-offset time, changes in the moveout of the dominant source, and perhaps of the drill-bit signal, should be apparent across that slice.

Figure 3.6 shows the velocity spectrum as a function of velocity and zero-offset time (the depth variable has been constrained to $v/2$). The moveout of the dominant source remains approximately constant despite variations in the depth of the drill bit in two depth intervals: from 300 m to 400 m, and from 780 m to 1 km.

Thus, average velocity spectra over time, as well as spectra shown as a function of time support the following three conclusions about the dominant source in the data: this source has a moveout independent from the depth of the drill bit; it operates continuously in time; and, it is most likely located at the surface, off the vertical plane containing the array.

3.1.3 Suppression of a strong source of noise by velocity filtering

To enhance the drill-bit signal with respect to the source of noise at the surface, I attenuate by dip-filtering the events in an interval of dips centered on the moveout of that surface source. Figure 3.7 shows the depth-velocity spectrum, computed after dip-filtering was

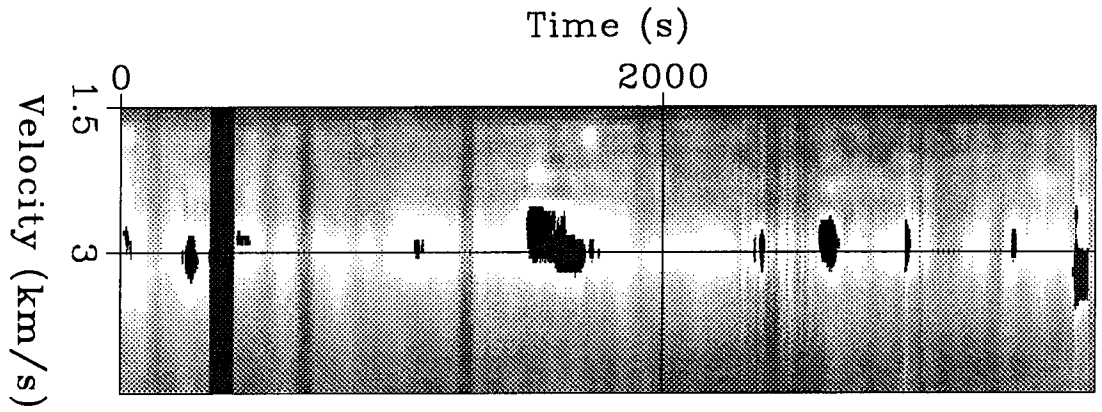

FIG. 3.6. Velocity-"zero-offset time" spectra for two intervals of borehole depths. The ratio of depth to velocity is kept constant for each record. The depth of the drill bit for records to the left of the black vertical stripe is around 400 m, while for records to the right of the stripe the depth increases from 770 m to 960 m.
The velocity of the dominant source in the data fluctuates around a constant value of 3 km/s. There is no indication of a trend of increasing velocity with depth, as expected from the drill-bit signal.

applied to the same 1 s long window of data as in Figure 3.3. The maximum of the energy in this spectrum is at the expected parameters for the signal from the drill-bit. However, a similar spectrum computed after the data in a 10 min long sequence had been dip-filtered, did not produce a maximum at the same expected parameters (Figure 3.8).

These results can be understood by referring to the signal and noise model inferred from previous depth-velocity spectra (Figures 3.5 and 3.4). Velocity filtering does enhance the drill-bit signal with respect to the source of noise at the surface; however, velocity filtering does not modify the signal-to-noise ratio between the drill-bit source and background noise with similar moveout. Therefore, the drill-bit signal becomes the dominant source after velocity filtering in the spectrum shown Figure 3.7 where the background noise is weak with respect to the drill-bit signal. However, when the background noise is stronger than the drill-bit signal, velocity filtering and velocity analysis fail to detect the drill-bit signal (Figure 3.8). As mentioned earlier, possible reasons for observing different signal-to-noise ratios in the 1 s long and in the 10 min long windows of data are differences in drilling conditions, or a better signal and noise separation in shorter window of data.

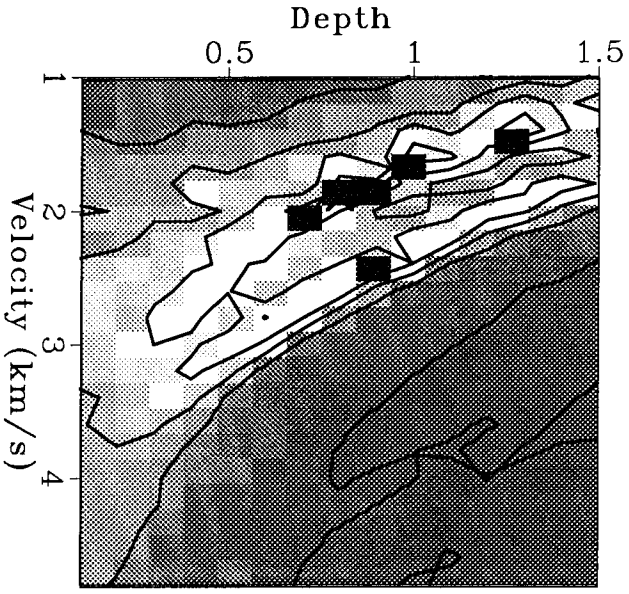

FIG. 3.7. Power of stack as a function of depth and velocity after suppression of the surface source for a 1 s window of data (same as in Figure 3.3). The maximum values indicated by black squares are at the expected moveout for signal from the drill bit: depth of 0.8 km and velocity of 1.9 km/s.

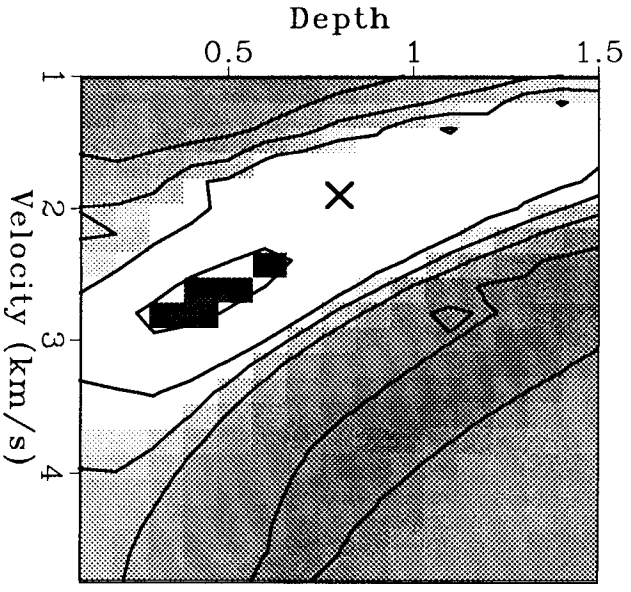

FIG. 3.8. Power of stack as a function of depth and velocity after suppression of the surface source for a sequence of data about 10 minutes long. The maximum values indicated by black squares do not appear at the expected moveout for signal from the drill bit.

3.2 Signal enhancement by cross-correlation

3.2.1 Introduction

In this section, I continue the separation of signal and noise by cross-correlation of the surface array data with a reference signal from a geophone located in a shallow borehole. The two main benefits anticipated from the cross-correlation are (1) the compression of the signal and noise waveforms into non-overlapping time-windows, and (2) the attenuation of certain types of noise, that are present on only one of the two channels being cross-correlated. I show with a theoretical model and with data examples how these effects depend on the length of the data sequence being cross-correlated. After cross-correlation, I measure the moveout of the coherent events by applying the methods for velocity analysis discussed earlier in this chapter.

3.2.2 Model of the cross-correlated seismograms

Let $\mathrm{Geo}(Z,T)$ denote the Z transform of the reference signal computed in a time-interval indexed by T. The following equation expresses the reference signal as the sum of drill-bit signal $\mathrm{Bit}(T,Z)$, and of a noise field $\mathrm{Noise}(Z,T,x_0,z_0)$ recorded at the location (x_0,z_0) of the reference geophone:

$$\mathrm{Geo}(Z,T) \;=\; \mathrm{Bit}(Z,T) \;+\; \mathrm{Noise}(Z,T,x_0,z_0). \tag{3.4}$$

The drill-bit signal at the reference geophone is the sum of a wavefield that has propagated directly from source to receivers (direct arrivals) and a scattered wavefield whose amplitude is typically smaller than 10% of the amplitude of the direct arrivals. In the subsequent analysis, I will neglect both the small-amplitude scattered wavefield, and the amplitude variations of the direct arrivals, because previous processing has repeatedly equalized amplitudes along offset.

Given the previous assumptions, the drill-bit signal recorded at the surface can be related to the drill-bit signal at the reference geophone by a simple traveltime delay $t(x,T)$. Therefore the model for the data recorded along the earth's surface, $\mathrm{Data}(Z,T,x)$, is:

$$\mathrm{Data}(Z,T,x) \;=\; \mathrm{Bit}(Z,T)Z^{t(x,T)} \;+\; \mathrm{Noise}(Z,T,x,0). \tag{3.5}$$

The traveltime delay $t(x,T)$ can also be expressed as a difference between the traveltimes along two paths — from the source to the receiver at the surface, and from the source to the reference geophone. In terms of the hyperbolic traveltime model (Equation 2.3.3), valid under the assumption of a horizontally layered medium, the traveltime delay becomes:

$$t(x,T) = \frac{\sqrt{x^2 + z^2}}{v(0)} - \frac{\sqrt{x_0{}^2 + (z - z_0)^2}}{v(z_0)}, \tag{3.6}$$

where $v(0)$ and $v(z_0)$ are respectively the RMS velocities at the surface and at the level of the reference geophone. In the right-hand side of the equation above, the depth z of the drill bit and the RMS velocities are implicitly functions of the time interval T.

The RMS velocity at depth z_0 is obtained by considering the traveltime delays for normal incidence:

$$\frac{z}{v(0)} = \frac{z - z_0}{v(z_0)} - \frac{z_0}{v_{\text{Near Surface}}}.$$

Because in the OGS experiment, the offset of the reference geophone x_0 is small the traveltime delay at that offset is approximately independent from the depth of the drill bit.

The noise field can also be decomposed into contributions of m sources, characterized by their wavelets $W_i(Z,T)$ and traveltime delays $n_i(x)$ with respect to the reference geophone:

$$\text{Noise}(Z,T,x,0) = \sum_{i=1}^{m} W_i(Z,T) Z^{n_i(x)}, \tag{3.7}$$

so that the model for the data (Equation 3.5) can be rewritten as:

$$\text{Data}(Z,T,x) = \text{Bit}(Z,T) Z^{t(x,T)} + \sum_{i=1}^{m} W_i(Z,T) Z^{n_i(x)}. \tag{3.8}$$

Noise that propagates as surface waves will be exponentially attenuated with depth (Aki and Richards, 1980). To include this effect, I model the noise at depth z_0 as

$$\text{Noise}(Z,T,x,z_0) = \sum_{i=1}^{m} |a_i|^{z_0} W_i(Z,T) Z^{n_i(x)}, \tag{3.9}$$

where a_i is a real number of magnitude less or equal than one.

The cross-correlation between the reference signal (Equation 3.4) and the surface array data (Equation 3.8) becomes then:

$$\begin{aligned} \text{Xcor}(Z,T,x) &= \text{Data}(Z,T,x)\text{Geo}(1/Z,T) = \\ &= |\text{Bit}(Z,T)|^2 Z^{t(x,T)} + \sum_{i=1}^{m} |a_i|^{z_0} |W_i(Z,T)|^2 Z^{n_i(x)} + \text{cross-terms.} \end{aligned}$$

3.2.3 Average cross-correlations

Assuming traveltime delays $t(x)$ that are approximately independent of T allows us to average the cross-correlated seismograms:

$$\begin{aligned} \text{Xcor}(Z,x) &= \left\{ \sum_T |\text{Bit}(Z,T)|^2 \right\} Z^{t(x)} + \sum_{i=1}^{m} \left\{ \sum_T |a_i|^{z_0} |W_i(Z,T)|^2 \right\} Z^{n_i(x)} + \\ &\quad + \text{cross-terms.} \end{aligned} \tag{3.10}$$

Averaging will have a different effect on each of the three components of the cross-correlation defined in Equation 3.10:

- Cross-terms, corresponding to the cross-correlation between sources that are incoherent in time, will be attenuated by averaging. The decrease in the energy of the cross-terms (an uncorrelated time series) will be proportional to the inverse of the length of the data sequence (Claerbout, 1985a).
- Components expressed in terms of autocorrelation functions[2] — drill-bit signal as well as noise — will be enhanced by averaging.

Because the moveout of the drill-bit signal varies as a function of depth, averaging will add constructively the low frequencies of that signal, while attenuating the high frequencies. The cut-off frequency $f_c(x)$ of the lowpass filter depends on offset, and can be expressed in terms of the maximum difference between traveltime delays as:

$$f(x) \leq f_c(x) = \frac{1}{t(x,T_{\min}) - t(x,T_{\max})}. \tag{3.11}$$

[2]Or, more rigorously, in terms of the Z transforms of autocorrelation functions.

Conversely, the above inequality can be used to restrict the length of the sequence of data being cross-correlated, so as to avoid cancellation of drill-bit signal.

The drill-bit signal and noise components that are enhanced in the average cross-correlation in Equation 3.10, are expressed as the convolution of a zero-phase wavelet (an autocorrelation) with a time-delay operator. Qualitatively, the time-duration of the zero-phase wavelet is related to the "smoothness" of its spectrum, and averaging cross-correlations will increase that smoothness. The shorter the time-duration of the wavelets, the easier it will be to separate the signal from the noise.

3.2.4 Examples of noise attenuation by cross-correlation

The anticipated effects from cross-correlation with a reference signal — attenuation of noise, and compression of the waveforms into non-overlapping windows — are illustrated in Figure 3.9.

The surface array data consist of a 25 s long window of data; coherent noise that propagates towards the well is clearly visible at the far offsets. Similar noise patterns were shown in Chapter 2, and attenuated by methods for signal and noise separation. The reference signal is recorded with a geophone located at 40 m depth at the offset nearest to the well. Because the coherent noise is not seen on the near offsets of the surface array, it is most likely not present at the reference geophone — located at 40 m depth at the offset nearest to the well — and therefore cross-correlation should attenuate such noise.

The cross-correlations before and after attenuation of coherent noise are compared in the top-right and bottom-left plots in Figure 3.9. Cross-correlation alone in 25 s long windows of data, without velocity filtering, is not sufficient to suppress the noise at the far offsets. To reduce computation time, velocity filtering could be applied also after cross-correlation and windowing in time, when the dataset is smaller.

The cross-correlation computed from a 10 min long sequence of data is displayed in the bottom-right plot of Figure 3.9. The noise at the far offsets propagating toward the well is eliminated. The events that are readily apparent on this seismogram are ground-roll noise with low apparent velocity at the near offsets, and strong noise with linear moveout at the far offsets.

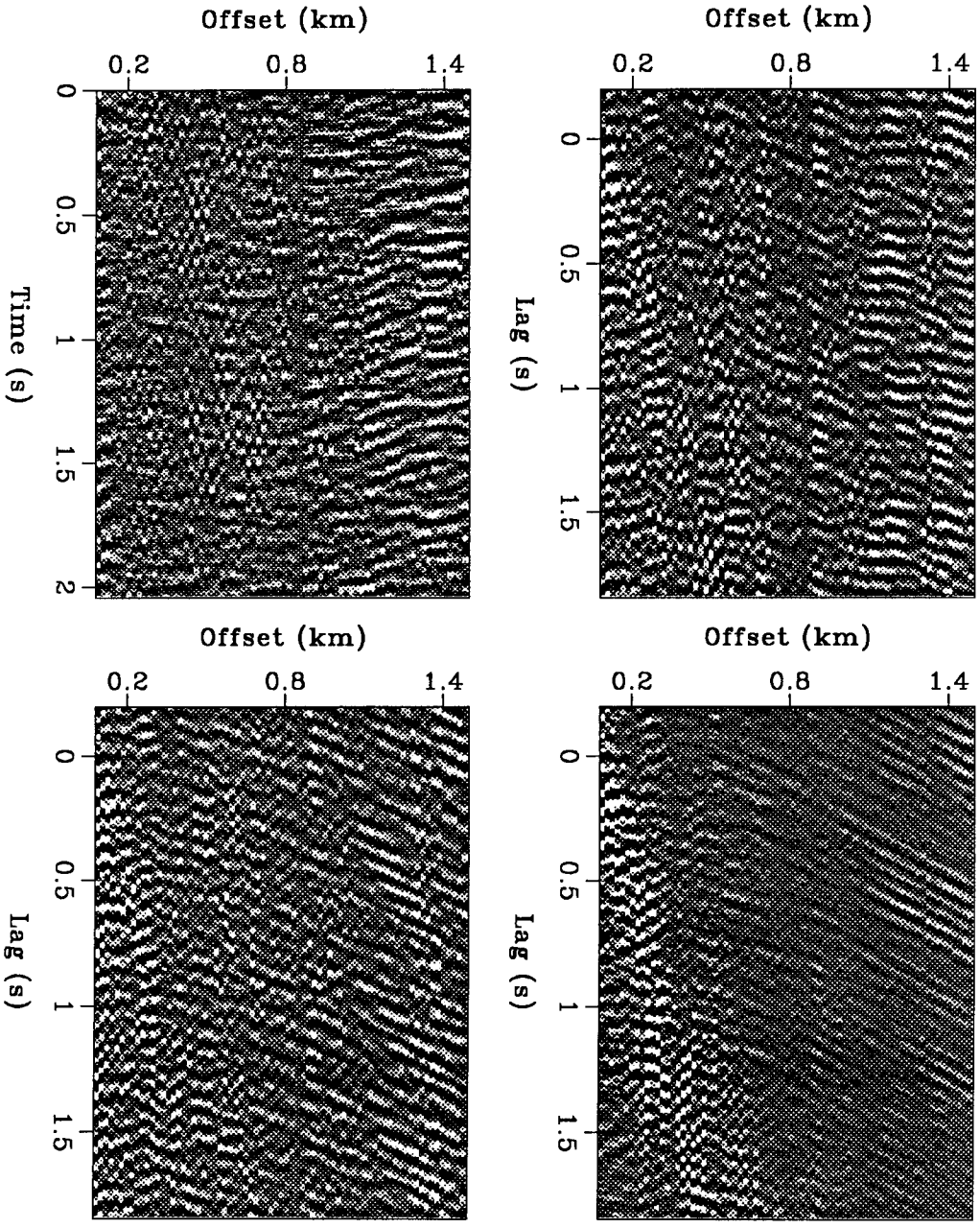

FIG. 3.9. Attenuation of coherent noise by cross-correlation.
Top row from left to right: (1) uncorrelated data with strong coherent noise at the far offsets; (2) cross-correlation computed *before* coherent noise attenuation from a 25 s long window of data.
Bottom row from left to right: (3) cross-correlation computed *after* coherent noise attenuation from a 25 s long window of data; (4) cross-correlation computed from a 10 min long sequence of data.
The cross-correlated seismograms computed from a 10 min long sequence of data, before or after velocity-filtering, appear identical on hardcopies.

3.2.5 Velocity analysis of cross-correlated data

The two characteristic properties of the moveout of signal from the drill bit are (1) hyperbolic traveltime delays, with parameters of the hyperbola given by the depth of the well and the stacking velocities from surface seismic data, and (2) a traveltime delay at near-offset equal to the time of propagation of an up-going wave from the buried reference geophone to the geophone at the surface and at the same offset. Both of these properties can be estimated from "zero-offset time"-velocity spectra, where the depth variable (Equation 3.2) is constrained to be constant.

In the computation of time-velocity spectra, it is possible to split the available data into sub-sequences, cross-correlate the data in each sub-sequence, and then average the time-velocity spectra computed from each sub-sequence. The longer the sub-sequence, the better the attenuation of cross-terms from time-incoherent sources. On the other hand, the statistical reliability of the average time-velocity spectrum increases with the number of spectra being averaged. For a given amount of data, there is a trade-off between having long sub-sequences, or having many sub-sequences. This trade-off is similar to the well-known trade-off between resolution and reliability in the computation of spectra of time series by the periodogram method (Claerbout, 1989; Marple, 1987).

The numerical examples presented below illustrate the effect of two extreme choices for the length of the data sequence being cross-correlated. First, I chose relatively short sub-sequences such that the lowpass effect on the drill-bit signal (Equation 3.11) would remain small at all offsets. Second, I cross-correlated all the data before computing the velocity spectrum.

A single velocity-spectrum computed from a long sequence of data

Figure 3.10 displays a seismogram and the corresponding velocity spectrum obtained by cross-correlation of the 50 min long sequence of surface array data with the signal from the geophone at depth of 40 m. The strongest events are either ground roll at the near-offsets, or their moveout is linear at the far offsets. The apparent velocity of the events with linear moveout is 1.75 km/s. The origin of these events is unknown; they might be refractions from sources at the surface.

Time-velocity spectra computed before or after the suppression of the events with linear moveout are shown in the right column of Figure 3.10. In each case, the ground-roll has

been muted before the computation of the velocity transform, and the depth parameter of the stacking trajectories is equal to 0.9 km. The time-velocity spectra obtained by this approach show the same events as the time-velocity spectra displayed later (for a smaller time-interval) in Figure 3.11.

The best evidence for drill-bit signal obtained thus-far is a weak event with a traveltime delay with respect to the reference signal of 0.072 s and velocity of about 1.9 km/s. This event is indicated with pointers in the time-offset and time-velocity domains on Figure 3.10. The hyperbolic event is not seen at the far offsets, either because of overlap with the strong noise having linear moveout, or because of differences in traveltime delays and the resulting lowpass effect.

Average of many velocity spectra

In this first approach to the computation of time-velocity spectra, I split a 50 min data sequence into 18 sub-sequences, each 3 min long. The change in the depth of the drill bit during each subsequence is less than 15 m (1/4 of wavelength at 30 Hz), and therefore the lowpass effect on the drill-bit signal should be small. The RMS velocities for the 50 min long data sequence are expected to increase from 1.88 km/s to 1.95 km/s.

Figure 3.11 displays time-velocity spectra for two different ranges of the time and velocity parameters, and for each of three reference signals, obtained from the vertical component geophones located at depths of 20, 40 and 60 m. The spectra are computed after muting of the ground-roll and suppression by dip-filtering of the events with linear moveout seen at the far offsets in the bottom-right panel of Figure 3.9.

The spectra, displayed for a large range of parameters, show that the dominant source in the cross-correlated data is narrowband with a dominant frequency of about 31 Hz, and that its apparent velocity is 2.5 km/s. This strongest source appears consistently on the spectra for each of the three reference geophones.

The spectra displayed for a smaller range of parameters around those expected for the dril-bit signal show significant local maxima only for the geophone at 40 m depth. The traveltime delays for these maxima are 0.044 s and 0.078 s; the traveltime of the second event is consistent with the previously determined traveltime of 0.072 s (Figure 3.10). The positive delays indicate that these events are up-going waves; the corresponding velocities of propagation in the near-surface are equal respectively to 0.9 km/s and to 0.5 km/s.

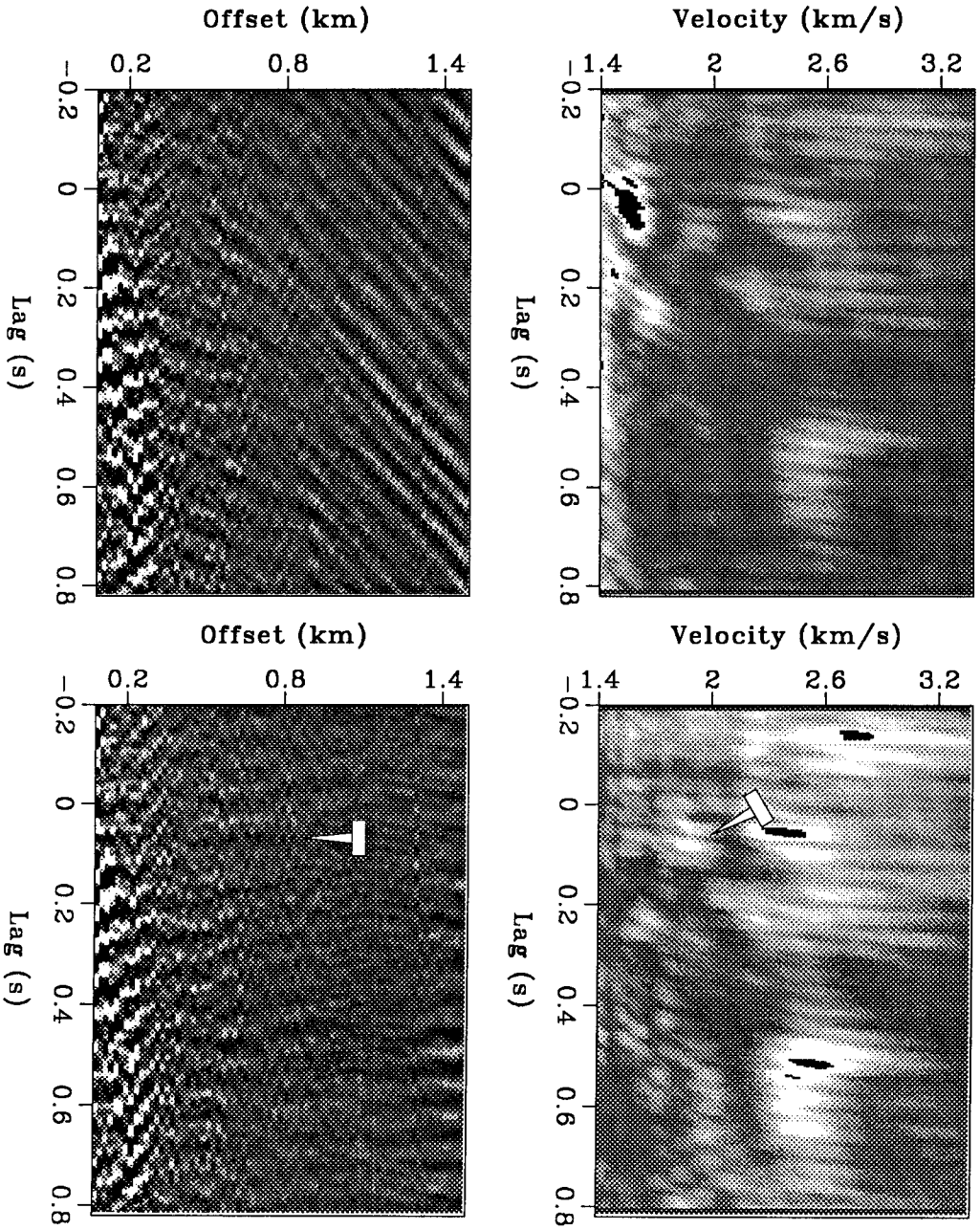

FIG. 3.10. Cross-correlation computed from a 50 min long data sequence (left column), and corresponding time-velocity spectra (right column) computed after the ground-roll has been muted.
The strong events with linear moveout, seen at far offsets in the top-left plot have been suppressed by dip-filtering (bottom-left panel) in order to emphasize events with hyperbolic moveout as expected from the drill-bit.
The seismogram in the bottom-left panel is displayed after moveout correction that should align direct arrivals from the drill bit. The parameters of the traveltime hyperbola are velocity equal to 1.9 km/s and depth equal to 0.9 km. The presumed drill-bit events are marked with pointers on the figures in the bottom row.

Either of these low velocities is plausible, because the near-surface layer is composed mainly of sands and shales.

Figure 3.12 shows variations in the velocity spectra as a function of recording time (or equivalently, depth of the drill-bit). For each of the 18 time-velocity spectra computed from the 3 min long data sequences, the energy was averaged in the interval of time from zero to 0.15 s. The three local maxima in that figure indicate an increase in the velocity with increasing depth of the well.

3.3 Summary of results and recommendations for future experiments

The dominant events in the raw data of the OGS experiment were narrowband noise, uncorrelated from trace to trace, and spatially correlated noise from sources at the surface, off the vertical plane containing the array. After signal and noise separation that enhanced the events over a range of moveouts centered around that expected for the drill-bit signal, coherent hyperbolic events became apparent in the data at about 15 db below the level of noise in the raw data. Stacking velocity analysis determined that the source of these events operates continuously in time and is located off the line of the array, most likely at the surface. Stacking velocity analysis also demonstrated that strong background noise with a broad dip-spectrum and power 3 db below the dominant source prevents the detection of the drill-bit signal.

The direct arrivals from the drill bit source were detected after cross-correlating the data from the surface array with a geophone at depth, and then averaging the velocity spectra or the cross-correlated seismograms over a 50 min long data sequence. Although the signal-to-noise ratios remain poor, this result provides interesting geophysical information. Knowledge of the moveout of the direct arrivals as function of offset and depth could be used for time-to-depth conversion of surface seismic data, and also for tomographic reconstruction of velocities around the borehole.

In retrospect, my recommendations for future surveys are the following:

- Sources of noise along the surface may be strong and invalidate the assumption of axial symmetry. Surface noise could be better detected and attenuated, if at least one more 1-D line, located on the surface and laid in a direction perpendicular to the first were available.

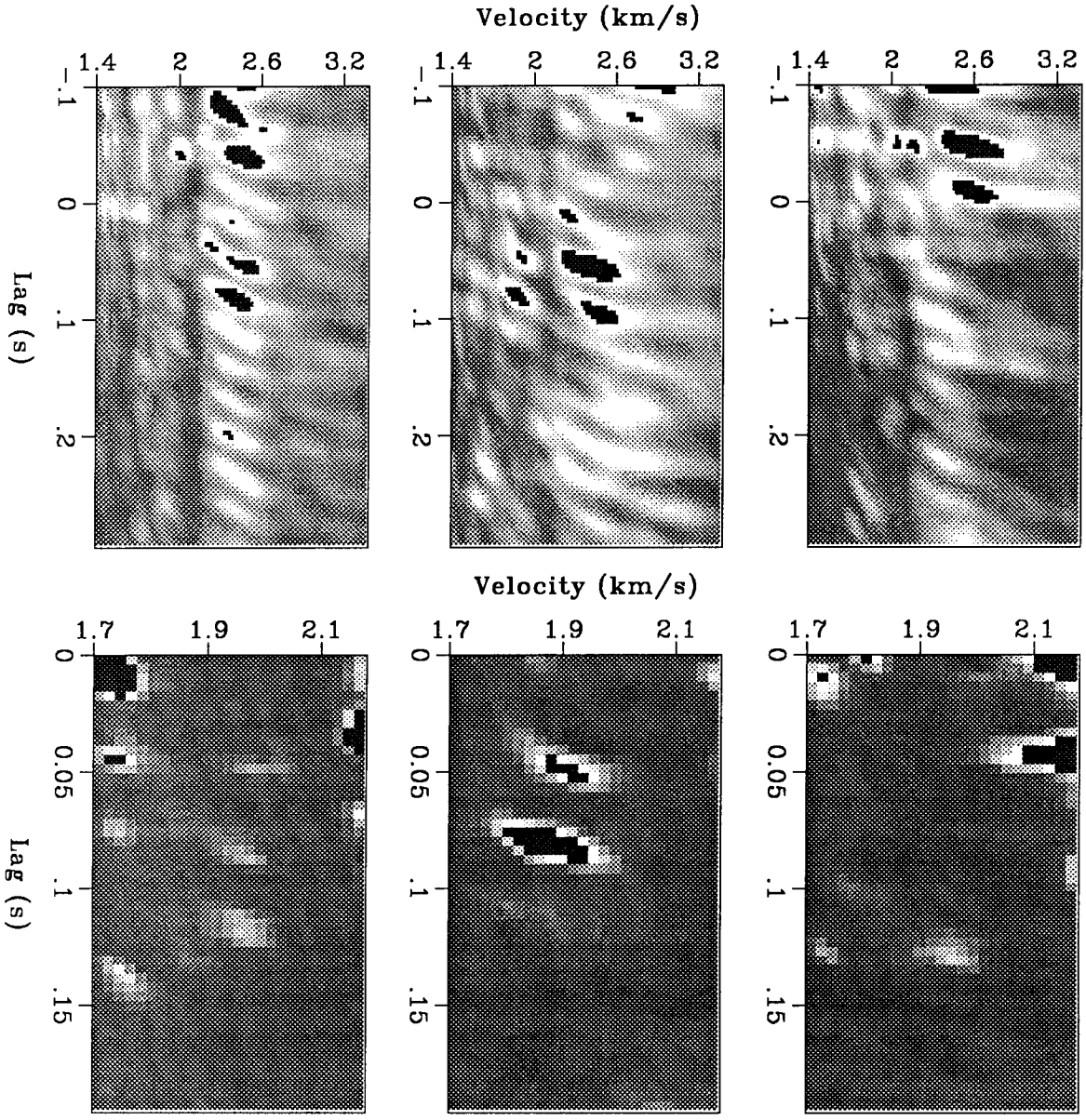

FIG. 3.11. Time-velocity spectra from surface array data cross-correlated with geophones at different depth levels of 20, 40, and 60 m. The depth of the reference geophone is the same for the spectra in each column, and increases from left to right.
The top row shows spectra for a large interval of time and velocity, while the bottom row shows only a small area of the spectrum around the expected location of the drill-bit signal. Events that could be attributed to the drill-bit source are seen only on the cross-correlation with the geophone at depth of 40 m.
The largest amplitudes above the 99^{th} percentile are clipped and appear as black areas surrounded by white.

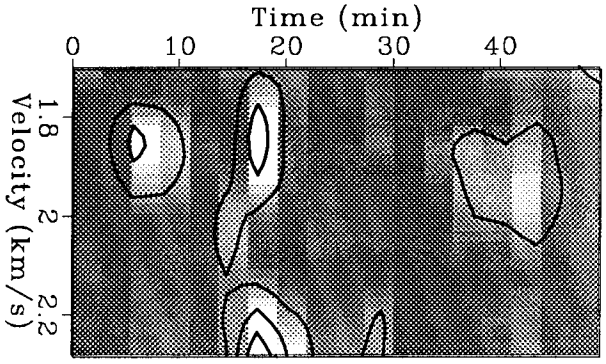

FIG. 3.12. Velocity spectra displayed as a function of the recording time. Each column in the plot is obtained by cross-correlation of a 3 min long data sequences, then computation of a "zero-offset time"-velocity spectrum, and finally averaging the energy in that spectrum over an interval of lags 0.15 s long centered on the expected traveltime delay for the drill-bit signal.
The velocity of the three local maxima, presumably generated by signal from the drill bit, increases with the increasing depth of the well.

- The idea of a vertical array in a nearby borehole is an original and promising one. However in the current experiment there were too few geophones in order to build an array, and to apply multichannel processing.

- Multichannel filtering separates signal and noise better than single channel filtering. I would recommend using the available channels to build arrays rather than recording reference signals.

- Records of ambient noise, made before drilling has started, could help to determine the level of ambient noise as well as its direction of propagation. Using that information, we could adapt the acquisition geometry to suppress such noise in the field.